JREE: Vol. 1, No. 1 (December 2014) 20-29

Research Article

Journal of Renewable Energy and Environment

Journal Homepage: www.jree.ir

Design of Innovative Channel Geometrical Configuration and Its Effect on Species Distribution

Ashkan Torkavannejad[*a], S. Mehdi Pesteei[a], Farzin Ramin[a], Nima Ahmadi[b], Hadi Shahmohammadi[c]

[a]*Department of Mechanical Engineering, Urmia University, Urmia, Iran*
[b]*Department of Mechanical Engineering, Urmia University of Technology,Urmia, Iran*
[c]*Department of Mechanical Engineering, Islamic Azad University of Tehran, Tehran, Iran*

Article History
Received:8 July 2013 Received in revised form: 26 Nov. 2013 Accepted: 3 Dec. 2013 Available online:17 Mar. 2014

A B S T R A C T

In this research, the impact of shoulder width and geometry of gas channel with different structures on proton exchange membrane (PEM) has been investigated using numerical method. 3D, non-isothermal was used with single straight channel geometrywhile maintaining the same boundary conditions and reaction area with addition of humidification for anode and cathode. Our study showed that an elliptical and circular channel cross-section gave higher current density as compared with conventional model. Moreover, the elliptical and circular channel configurations facilitated reactant transportation, caused more homogenous distribution of reactants andeffectively reduced mass transport loss, which lowered cathode overpotential of the cell which is the main cause of loss. Simulation of the three different channel geometries revealed that shoulder width has dominating effect on cell performance and leads to increase the value of Ohmicloss. The numerical model is validated against published experimental data and shows good agreement. Additional results with more detail are discussed and presented in the text.

Keywords: Channel Cross-Section, Fuel Cell Performance, PEM Fuel Cells, Single-Phase

1. Introduction

Fuel cells are electrochemical devices that change chemical energy of reactants, directly into electrical energy. The important features of fuel cell that sharply increased the appeal of fuel cells in generating electricity include: high performance, not being limited to Carnot cycle, silent and long term operation, and not having problems of emission control and waste disposal. These advantages make the fuel cells attractive choices for the replacement to internal combustion engines. High cost of launch and economical cost is the major disadvantage of fuel cells. Different types of fuel cells have been developed, which are distinguished by the electrolyte used. Among all kinds of fuel cells, proton exchange membrane fuel cell (PEMFC) has been considered as a principle candidate for future transportation application as well as for small devices such as laptop. In these fuel cells, fuel (e.g., hydrogen gas) and an oxidant (e.g., oxygen gas from the air) are used to generate electricity, while heat and water are unavoidable products of the fuel cell operation. A fuel cell typically works on the following principle: as the hydrogen gas flows into the fuel cell on the anode side, a platinum catalyst facilitates oxidation of the hydrogen gas which produces protons (hydrogen ions) and electrons. The hydrogen ions diffuse the MEA. The electrons, which cannot pass through the membrane, flow from the external electrical circuit for energy consumption. At the cathode side, oxygen molecules combine with hydrogen ions and produce water and heat. The anode and the

[*] Corresponding author. *Email: ashkantorkavannejad@yahoo.com*

cathode (the electrodes) are porous and made of an electrically conductive material, typically carbon. The faces of the electrodes in contact with the membrane contain. The PEM electrodes are kind of gas-diffusion type and generally designed for maximum surface area per unit material volume.

In recent years, researchers pay more attention to modeling and simulation of different aspects in PEMFCs with a view to enhance the cell performance and optimize the cost. In this way, a great number of researches have been conducted to improve the performance of PEMFC. Among these studies, various operating condition have been examined [1-9].Another major issue that researchers focus more for commercialization of these cells, is the geometrical design of PEMFC. One of the geometrical parameters that affect the fuel cells is the shoulder width. It has been found that cells with smaller shoulder width are better than those with larger shoulder width due to more uniformdistribution of reactants [10-13]. Other geometries have been investigated to increase permeability of reactants by using obstacle in the channel area [14] and different channel geometries [15-18]. Various serpentine flow fields have been examined for reaching higher output [19-21]. Ahmed et al. [22] performed simulations of PEMFCs with a new design for the channel shoulder geometry, in which the MEA is deflected from shoulder to shoulder. Arabi et al. [23] investigated the effect of an innovative bipolar plate on PEMFC performance. Pourmahmoud et al. [24] investigated the gas diffusion layer thickness effect on PEMFC performance; they also worked on the impact of structural parameters of bipolar plates on the PEMFC performance [25].

In the present study, three-dimensional, single phase, isothermal and parallel flow model of a PEM fuel cell with different channel geometries were performed, which the inlet area is constant in both anode and cathode side. These geometries were used with single straight channel geometry while maintaining the same boundary conditions and inlet area,and including humidification for both anode and cathode.

These new geometries were designed to improve the reactant distribution and improve the cell performance.

The numerical results showed that geometries with circular and elliptical channel give higher current density at the same voltage compared to conventional channels because of the effective and uniform distribution of the reactants on the reacting area, and having less cathode over potential which is the main source of loss in PEMFC.

The simulation results were validated by comparison with results in the literature and showed good concord with experimental data. Detailed analyses of the fuel cell behavior under various geometries are discussed in the following sections.

2. Model description

2.1. System description

Constant mass flow rate at the channel inlet, constant pressure condition at the channel outlet, and no-flux conditions are executed for mass, momentum, species and potential conservation equations at all boundaries expect for inlets and outlets of the anode and cathode flow channels.

The side faces are symmetrical, while in the experimental sets, the fuel cell has three mono cells. For the layers where the electrochemical reactions occur the meshes are finer. Also, grid independence test was implemented, and finally the optimum number of meshes (164 000) was chosen. Figure 1 indicates the computational domain of base model. The cell consists of hydrogen and oxygen channels, bipolar plates on cathode and anode side of cell, which function as current collector with high electronic conductivity, and the membrane electrode assembly (MEA) is located between gas channels.

2.2. Model assumptions

Non-isothermal model is assumed to perform in steady manner under constant load conditions. All gases are assumed to obey ideal gas behaviors. GDLs and catalyst layers are homogeneous and isotropic porous mediums. Flow is incompressible and laminar due to the low pressure gradients and velocities. Volume of liquid-phase water produced in electrochemical reactions is negligible and phase change or two phase-transports are not considered; so, this model is considered as a single phase. The membrane is impermeable to cross-over of reactant gases and assumed to be fully humidified. The species diffusion and electrochemical reaction conform to the dilute solution theory and Butler-Volmer kinetic equation, respectively.

3. Model equations

3.1. Gas flow fields

In the fuel cell, the gas-flow field is obtained by solving the steady-state Navier-Stokes equations, i.e. the continuity equation:

$$\nabla.(\rho u) = 0 \quad (1)$$

and momentum equations;

$$\nabla .(\rho u \otimes u - \mu \nabla u) = - \nabla (P + \frac{2}{3} \mu \nabla u) + \nabla .\left[\mu (\nabla u)^T \right] \quad (2)$$

The mass balance is described by the divergence of the mass flux through diffusion and convection. The steady state mass transport equation can also be written in the following expression for species i:

$$\nabla .\left[-\rho y_i \sum_{j=1}^{N} D_{ij} \frac{M}{M_j} \left(\nabla y_j + y_j \frac{\nabla M}{M} \right) + \rho y_i u \right] = 0 \quad (3)$$

where the subscript i denotes oxygen at the cathode side, and hydrogen at the anode side, and j is water vapor in both cases. Nitrogen is the third species at the cathode side.

The Maxwell-Stefan diffusion coefficients of any two species are dependent on temperature and pressure. They can be calculated according to the empirical relation based on the kinetic gas theory [23];

$$D_{ij} = \frac{T^{1.75} \times 10^{-3}}{P\left[\left(\sum_k V_{ki} \right)^{1/3} + \left(\sum_k V_{kj} \right)^{1/3} \right]^2} \left[\frac{1}{M_i} + \frac{1}{M_j} \right]^{1/2} \quad (4)$$

In this equation, pressure is in [bar], and the binary diffusion coefficient is in [cm^2/s]. The values for $\sum V_{ki}$ are given by Fuller et al. [25], and the temperature field is obtained by solving the convective energy equation;

$$\nabla .(\rho C_p u T - k \nabla T) = 0 \quad (5)$$

3.2. Gas diffusion layers

Transport in the gas diffusion layer is modeled as transport in a porous media. The continuity equation in the gas diffusion layers becomes:

$$\nabla .(\rho \varepsilon u) = 0 \quad (6)$$

The momentum equation reduces to Darcy's law:

$$u = \frac{Kp}{\mu} \nabla P \quad (7)$$

The mass transport equation in porous media is:

$$\nabla .\left[-\rho \varepsilon y_i \sum_{j=1}^{N} D_{ij} \frac{M}{M_j} \left(\nabla y_j + y_j \frac{\nabla M}{M} \right) + \rho \varepsilon y_i u \right] = 0 \quad (8)$$

In order to account for geometric constraints of the porous media, the diffusivities are corrected using the Bruggeman correction formula:

$$D_{ij}^{eff} = D_{ij} \times \varepsilon^{1.5} \quad (9)$$

The heat transfer in the gas diffusion layers is governed by:

$$\nabla .(\rho \varepsilon C p u T - k_{eff} \varepsilon \nabla T) = \varepsilon \beta (T_{solid} - T) \quad (10)$$

where, the term on the right-hand side accounts for the heat exchange to and from the solid matrix of the GDL. Here, β is a modified heat transfer coefficient that accounts for the convective heat transfer in [W/m^2] and the specific surface area [m^2/m^3] of the porous medium [26]. Hence, the unit of β is [W/m^3]. The potential distribution in the gas diffusion layers is:

$$\nabla .(\lambda_e \nabla \phi) = 0 \quad (11)$$

3.3. Catalyst layers

The catalyst layer is treated as a thin interface, where sink and source terms for the reactants are implemented. Due to the infinitesimal thickness, the source terms are actually implemented in the last grid cell of the porous medium. At the cathode side, the sink term for oxygen can be written as:

$$S_{o_2} = - \frac{M_{o_2}}{4F} i_c \quad (12)$$

Whereas, the sink term for hydrogen is specified as:

$$S_{H2} = -\frac{M_{H_2}}{4F} i_a \quad (13)$$

The production of water is modeled as a source terms and hence can be given as:

$$S_{H_2O} = \frac{M_{H_2O}}{2F} i_c \quad (14)$$

The generation of heat in the cell is due to entropy changes as well as irreversibility due to the activation over potential:

$$\dot{q} = \left[\frac{T(-\Delta s)}{n_e F} + \eta_{act,c} \right] i_c \quad (15)$$

The local current density distribution in the catalyst layers can be modeled by the Butler-Volmer equation:

$$i_c = i_{o,c}^{ref}\left(\frac{C_{o_2}}{C_{o_2}^{ref}}\right)\left[\exp\left(\frac{\alpha_a F}{RT}\eta_{act,c}\right)+\exp\left(-\frac{\alpha_c F}{RT}\eta_{act,c}\right)\right] \quad (16)$$

$$i_a = i_{o,a}^{ref}\left(\frac{C_{H_2}}{C_{H_2}^{ref}}\right)^{0.5}\left[\exp\left(\frac{\alpha_a F}{RT}\eta_{act,a}\right)+\exp\left(-\frac{\alpha_c F}{RT}\eta_{act,a}\right)\right] \quad (17)$$

3.4. Membrane

The balance between the electro-osmotic drag of water from anode to cathode and back diffusion from cathode to anode yields the net water flux through the membrane:

$$N_W = n_d M_{H_2O}\frac{i}{F} - \nabla(\rho D_w \nabla y_w) \quad (18)$$

For heat transfer purposes, the membrane is considered a conducting solid, which means that the transfer of energy associated with the net water flux through the membrane is neglected. Heat transfer in the membrane is governed by:

$$\nabla.(k_{mem}\nabla T) = 0 \quad (19)$$

The potential loss in the membrane is due to resisting to proton transport across membrane which is equal to:

$$\nabla.(\lambda_m \nabla \phi) = 0 \quad (20)$$

3.5. Boundary conditions

For the momentum conservation equation, fuel velocity is specified at each inlet of anode and cathode flow channel. The velocity is calculated based on the concept of stoichiometry, which means "the required amount of fuel at a given condition". Boundary conditions are set as follows: constant mass flow rate at the channel inlet and constant pressure condition at the channel outlet. The inlet mass fractions are determined by the inlet pressure and humidity according to the ideal gas law. Gradients at the channel exits are set to zero. The equations for both inlets are expressed as:

$$|\vec{u}|_{in} = \frac{\zeta}{X_{H_{2,in}}}\frac{I_{avg}}{2F}\frac{RT_{in}}{P_{in}}\frac{A_{MEA}}{A_{ch}} \quad (21)$$

I_{avg} is the average current density at a given cell-potential. Where, R, T_{in}, P_{in}, and ζ are the universal gas constant, temperature in the inlet, pressure in the inlet, and stoichiometric ratio, respectively. The latter is defined as the ratio between the amount of supplied and the amount of required reactant on the basis of the reference current density I_{avg}, accordingly.

4. Numerical implementations

For solving the equations, the simple algorithm is applied. In addition, the main procedure for discretizing the governing equations with the appropriate boundary conditions is finite volume method and implicit solver. Figure 2 shows the algorithm for numerical simulation of model equations.

Numerical test results were performed to ensure that the solutions were independent of the grid size. Moreover, the computational domain is divided into about 164,000 cells.

5. Results and Discussion

To validate the numerical simulation model used in the present study, the polarization curves were compared with the experimental data presented by Wang et al. [28]. Polarization curve of present model is shown in Figure 3. This curve signifies good concord between numerical model and experimental data. Different types of over potentials and losses are depicted in Figure 4 which is a function of current density. Proposed models were chosen with the same reactant flow rate and constant boundaryconditions. The fully humidified inlet condition for anode and cathode is used. Parametric and operating conditions can be found in Table 1.

In order to improve conventional cell performance by improving the distribution of reactants over the GDL, we simulated three kinds of channel geometries in which the cross sections of channel changed to circular and ellipticalfor decreasing the effect of concentration losses or mass transport limitations is depicted in Figure 5.Geometry of proposed models is presented in Table 2.

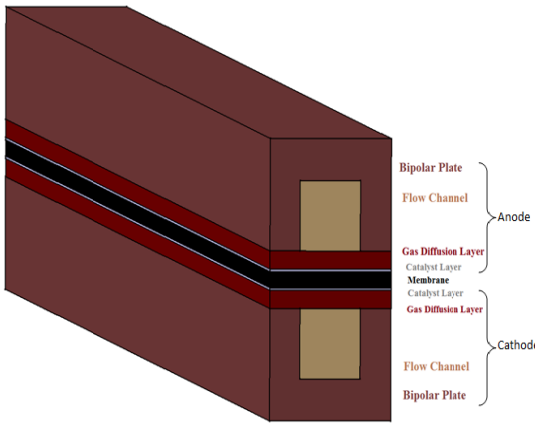

Fig.1. Computational domain of base model

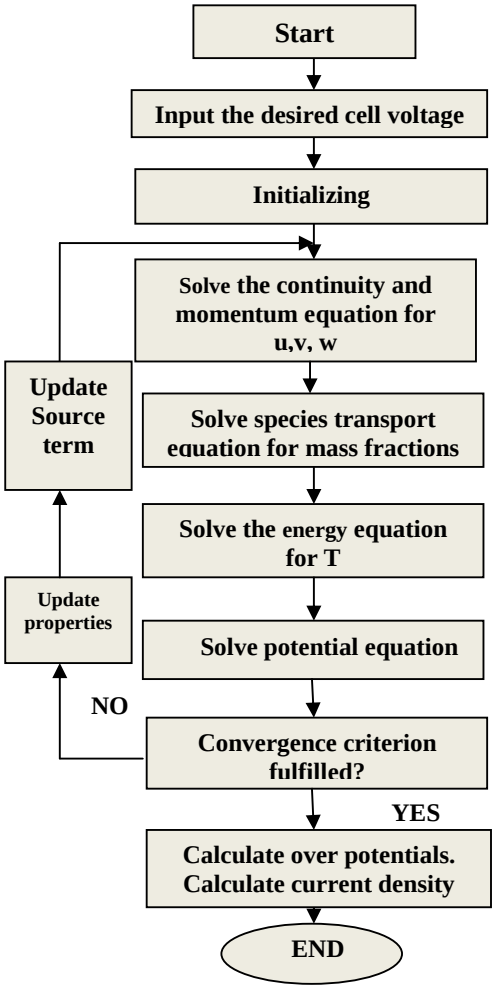

Fig.2. The algorithm for numerical simulation

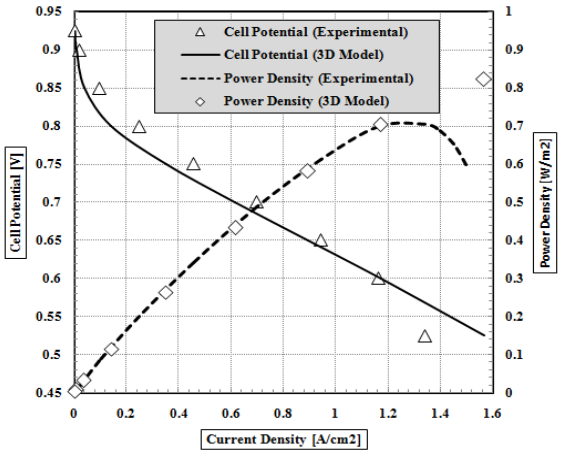

Fig.3. Comparison of polarization curve of model with experimental data

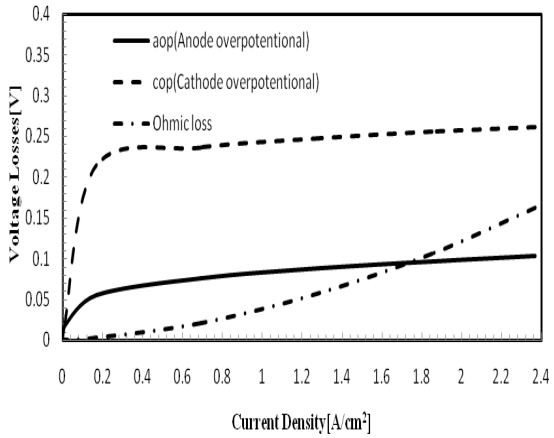

Fig. 4. Different types of voltage losses for the base case

Table 1. Geomerric paramets and operation conditions

Parameters	Value	Unit
Channel length	0.05	m
Channel width	1e_3	m
Channel height	1e_3	m
Land area width	1e_3	m
Gas diffusion layer thickness	0.26e_3	m
Catalyst layer thickness	0.0287e_3	m
Wet membrane thickness	0.23e_3	m
Anode and Cathode pressure	3	atm
Inlet air and fuel temperature	353.15	k

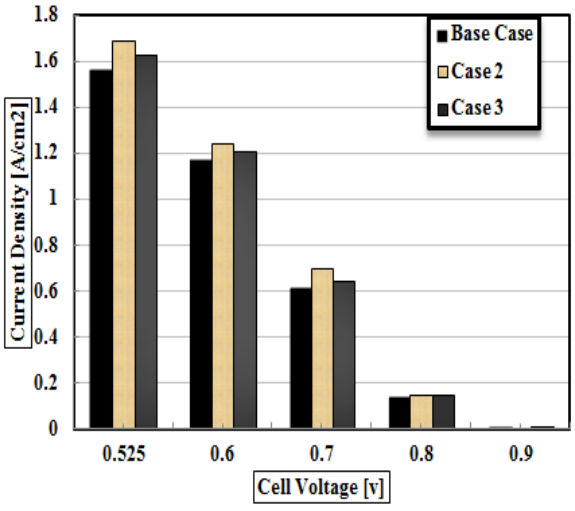

Fig.6.Comparison of performance of three numerical cases

The numerical results show that the case with elliptical geometry (case 2) produces more current density than the conventional and circular (case 3) models at the same cell voltage (Figure 5).

Providing reactants is an important factor for improving fuel cells performance; in this way, oxygen distribution and counters are depicted in Figures 7and 8.

It can be concluded that these new geometries intensify the oxygen transportation to the GDL at shoulder area, which in cases 2 and 3 mass fraction is higher at the shoulder area and more uniform. This makes it easier for reactants to diffuse through the GDL and increase oxygen utilization efficiency, but in case 1(base), this phenomenon is completely reverse. In case 1, lack of oxygen at the cell shoulder

regions causes higher reactant shortage than the cases 2 and 3.

The figures show that the dependency of reactants attributes to channel geometries. This observation indicates that new geometries have high efficacy in transportation of reactants to the reaction area. Oxygen accumulation decreases gradually along the flow channel due to the consumption, but at base case oxygen scarcity in the shoulder region over the reacting area leads to higher concentration losses, which becomes worse in downstream region of the channel due to depletion of reactants with moving downstream.

At the catalyst layer, the accumulation of oxygen is balanced by consuming the oxygen and the amount of oxygen that penetrates towards the catalyst. The lower diffusivity of the oxygen along the flow is dueto the presence of water in the pores of the cathode catalyst layer.

At the catalyst layer, the accumulation of oxygen is balanced by consuming the oxygen and the amount of oxygen that penetrates towards the catalyst. The lower diffusivity of the oxygen along the flow is due to the presence of water in the pores of the cathode catalyst layer.

Results show that significant losses of the cell voltage occur at the cathode side. COP causes to increase the activation and concentration losses at the cathode side. Inspection of the cop distribution in the fuel cell is shown in Figure 9. The cathode over potential is mainly affected by the oxygen accessibility at the membrane–cathode GDL interface, which increases significantly in the shoulder region as well as in the downstream region of the channels.

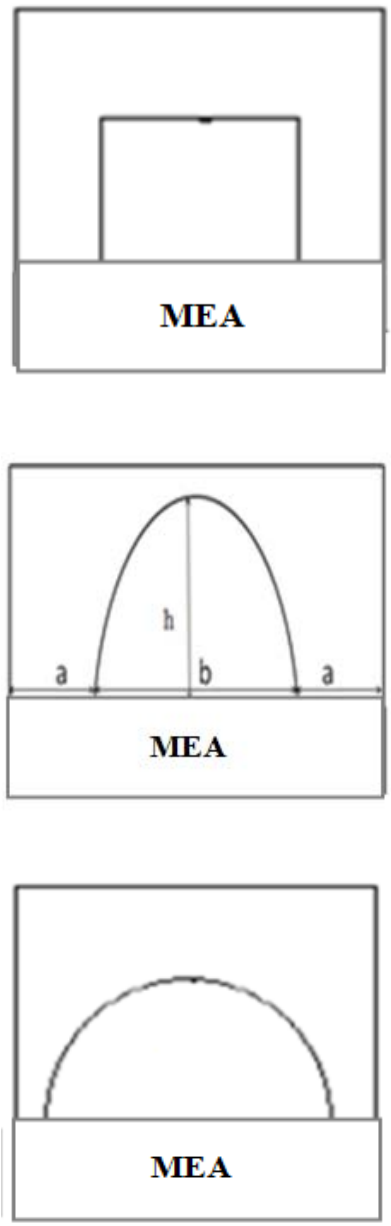

Fig. 5. Conventional and new geometries with elliptical and circular gas channel at cathode and anode side.

The distribution of oxygen mass fraction at the membrane–cathode catalyst interface is shown in Figures 7 and 8. In case 1, oxygen shortage in the shoulder region over the reacting area leads to higher activation losses which becomes worse in the downstream region of the channel due to depletion of the reactant with moving downstream, but in cases 2 and 3 this condition is completely reverse due to different oxygen distribution.

Table 2. Geometrical configuration

Case	Channel width (mm) (b)	shoulder width (mm) (a)	channel height (mm) (h)	reacting area (cm²)
Conventional	1	0.5	1	1
Elliptical	1.2	0.4	0.53	1
Circular	1.6	0.2	0.8	1

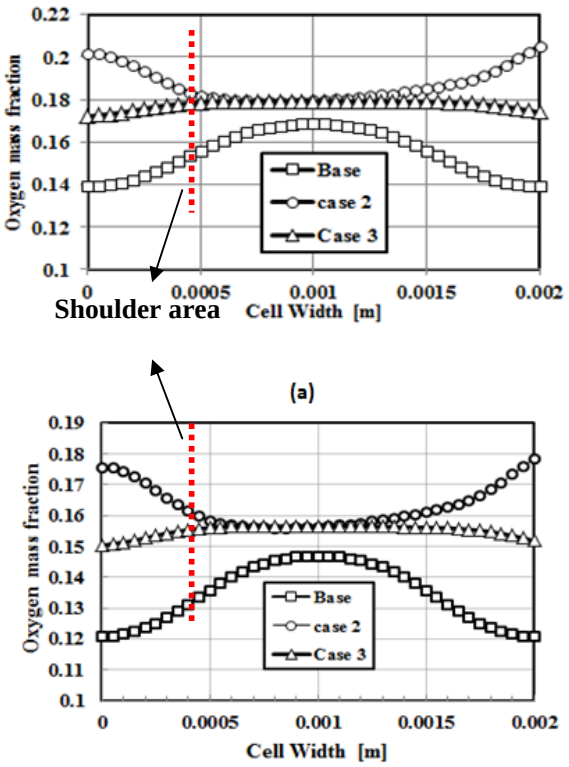

Fig.7. Comparison of oxygen mass fraction at the interface of membrane and cathode catalyst layer for three numerical models at entry (a), and exit (b) region at same voltage (0.6 volt).

One of the important parameters that reduce oxygen diffusivity is water. Usually, at high operating current densities, more molecules react, and therefore more water is produced, which reduces the oxygen diffusivity in the cell. All in all, among the three cases considered here, cases 2 and 3 due to high value of oxygen and uniform distribution, show lower COP in both channel and shoulder area.

Due to lower COP in the new configurations, it can be concluded that there is no critical oxygen scarcity. Ohmicloss is attained by multiplying the Ohmicresistance and current density. Hence, Ohmicloss is directly related to the membrane thickness, tm, local current density, I, and inversely related to the membrane conductivity, σe. The simulation results point out that Ohmicloss is higher in the channel area than in shoulder area (Figure 10) and proved that the configuration with a larger channel width and smaller shoulder (case3) experiences higher Ohmiclosses.

6. Conclusions

In the present work, we made simulations of a PEMFC with single straight channel geometrywith the intention of being practical and extendable for other fuel cells with any dimensions and structural and operating parameters. The result of simulation using these channel geometries revealed that the circular and elliptical channel cross-sections gives higher current density. Also, the oxygen distribution is more uniform in new geometries which the value of COP has direct linkage with oxygen. Moreover, the results imply that the cathode over potential was sensitive to the shoulder width and oxygen distribution, which in case 2, the reactants transportation to the GDL is more than the others.

Comparing these two losses for the three cases, it is concluded that the Ohmicloss and COP had powerful effect in reducing the fuel cell performance. Implementation of these new geometries yields more homogenous and reduced mass transport loss, as well as favoring a uniform

distribution over active area and homogenous current production and high cell performance.

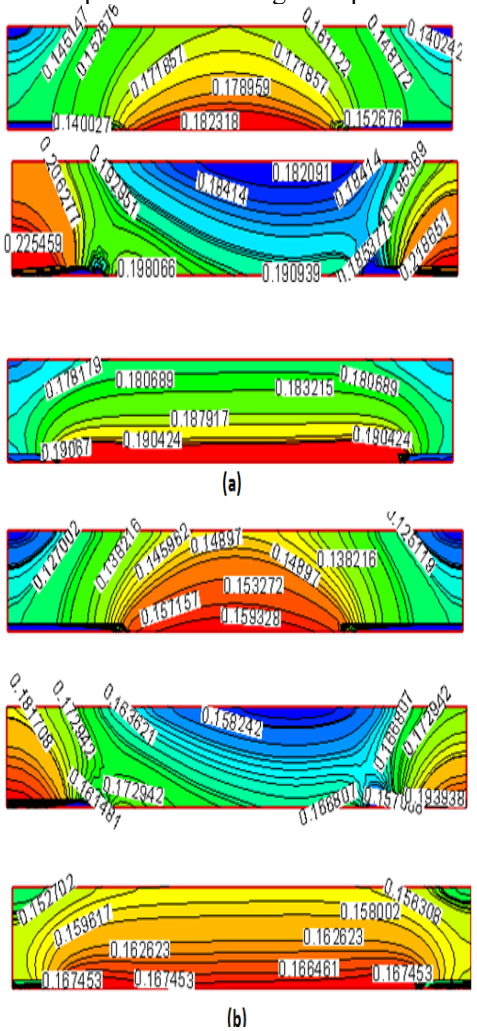

Fig. 8. Contours of oxygen mole fraction at the catalyst layer and gas diffusion layer of cathode for different deflection at entry (a), and exit (b) region (0.6 volt) (base, elliptical and circular respectively).

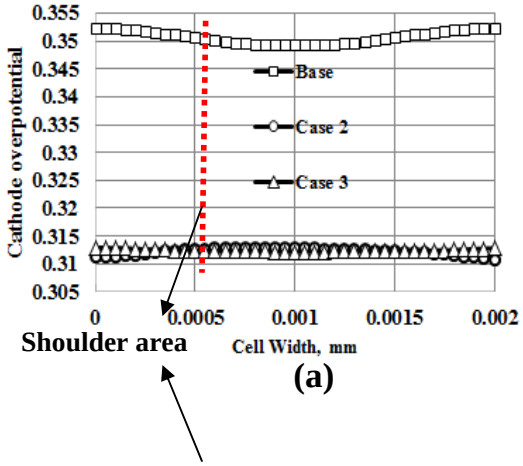

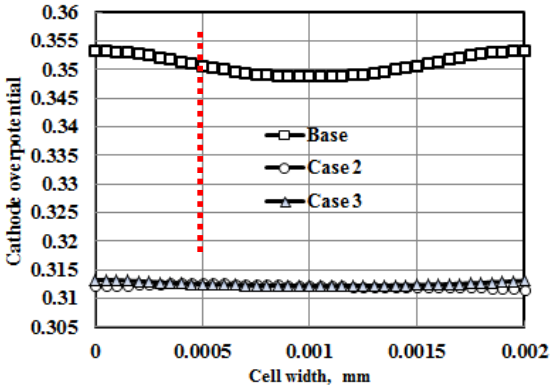

Fig. 9. Comparison of COP at the interface of membrane and cathode catalyst layer for three numerical models at entry (a) and exit (b) region at the same voltage (0.6 volt).

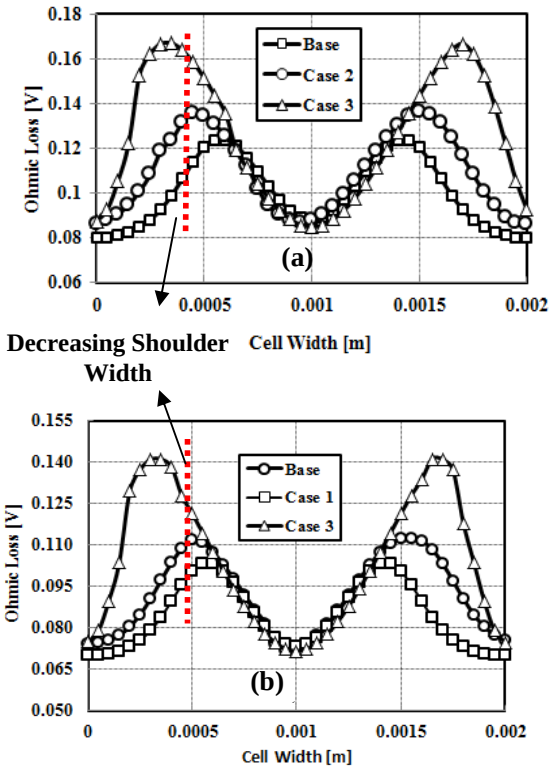

Fig. 10. Comparison of Ohmic loss at the interface of membrane and cathode catalyst layer for three numerical models at entry (a) and exit (b) region at same voltage (0.6 volt).

7. Acknowledgment

The financial support of the Renewable Energy Organization of Iran is gratefully acknowledged [SUNA].

8. Nomenclature

a	Water activity
C	Molar concentration (mol/m^3)
D	Mass diffusion coefficient (m^2/s)
F	Faraday constant (C/mol)
I	Local current density (A/m^2)
J	Exchange current density (A/m^2)
K	Permeability (m^2)
M	Molecular weight (kg/mol)
nd	Electro-osmotic drag coefficient
P	Pressure (Pa)
R	Universal gas constant (J/mol-K)
T	Temperature (K)
t	Thickness
V	Cell voltage
Voc	Open-circuit voltage
W	Width
X	Mole fraction

Greek Letters

α	Water transfer coefficient
εeff	Effective porosity
ρ	Density (kg/m^3)
μ	Viscosity (kg/m-s)
σe	Membrane conductivity (1/ohm-m)
λ	Water content in the membrane
ζ	Stoichiometric ratio
η	Over potential (v)
λ_{eff}	Effective thermal conductivity(w/m-k)

Subscripts and Superscripts:

a	Anode
c	Cathode
cl	Catalyst
GDl	Gas diffusion layer
ch	Channel
k	Chemical species
m	Membrane
MEA	Membrane electrolyte assembly
ref	Reference value
sat	saturated
w	Water

9. References

1. Xing X.Q., Lum K.W., Poh H.J., Wu Y.L. Optimization of assembly clamping pressure on performance of proton-exchange membrane fuel cells. J Power Sour, 2010, 195, 62-68.
2. Chang W.R., Hwang J.J., Weng F.B., Chan S.H. Effect of clamping pressure on the performance on a PEM fuel cell. J Power Sour, 2007, 166, 149-154.
3. Rho Y., Rho Y.W., Velev O. A., Srinivasan S., Kho Y.T. Mass transport in protonexchange membrane fuelcells using O2/H2, O2/Ar and O2/N2 mixtures. J Electrochem Soc, 2003, 141, 38-45.
4. Amphlett J.C., Baumert R.M., Mann R.F., Peppley B.A., Roberge P.R., Harris T.J. Performance modeling of the ballard mark IV solid polymer electrolyte fuel cell. J Electrochem Soc, 1995, 142(1), 16-19.
5. Mosdale R., Srinivasan S. Analysis of performance and of water management in proton exchange membrane fuel cells. Electrochem Acta, 1995, 40, 413-421.
6. Oetjen H.F., Schmidt V.M., Stimming U., Trila F. Performance data of a proton exchange membrane fuel cell using H2/Co as fuel gas. J Electrochem Soc, 1996, 143, 38-42.
7. Buchi F.N., Srinivasan D. Operating proton exchange membrane fuel cells without external humidification of the reactant gases. J Electrochem Soc, 1997, 144, 27-67.
8. Uribe F.A., Gottesfeld S., Zawodzinski T.A. Effect of ammonia as potential fuel impurity on proton exchange membrane fuel cell performance. J Electrochem Soc, 2002, 149, 293-296.
9. Ticianelli E.A., Derouin C.R., Srinivasan S. Localization of platinum in low catalyst loading electrodes to attain high power densities in SPE fuel cells. J Electro Anal Chem, 1988, 251, 275-295.
10. Natarajan D.T., Nguyen V. A two-dimensional, two-phase, multicomponent, transient model for the cathode of a proton

exchange membrane fuel cell using conventional gas distributors. J Electrochem Soc, 2001, 148(12), 1324–1335.
11. Lin G., Nguyen T.V. A two-dimensional two-phase model of a PEM fuel cell. J Electrochem Soc, 2006, 153(2), 372–382.
12. Lum K.W., McGuirk J.J. Three-dimensional model of a complete polymer electrolyte membrane fuel cell–model formulation, validation and parametric studies. J Power Sour, 2005, 143, 103–124.
13. Ahmed D.H., Sung H.J. Effects of channel geometrical configuration and shoulder width on PEMFC performance at high current density. J Power Sour, 2006, 162, 327–339.
14. Ahmadi N., Rezazadeh S., Mirzaee I., Pourmahmoud N. Three-dimensional computational fluid dynamic analysis of the conventional PEM fuel cell and investigation of prominent gas diffusion layers effect. J Mech Sci Tech, 2012, 12(8), 1-11.
15. Ge S., Yi B.A. Mathematical Model for PEMFC in Different Flow Modes. JPower Sour, 2003, 124(1), 1-11.
16. Sun L., Oosthuizen P.H., McAuley K.B. A Numerical Study of Channel-to-Channel Flow Cross-over Through the Gas Diffusion Layer in a PEM-fuel-cell Flow System Using a Serpentine Channel with a Trapezoidal Cross-sectional Shape. Int J Therm Sci, 2006, 45(10), 1021-1026.
17. Guvelioglu G.H., Stenger H.G. Computational Fluid Dynamics Modeling of Polymer Electrolyte Membrane Fuel Cells. J Power Sour, 2005, 147(9), 95-106.
18. Chiang M.S., Chu H.S. Numerical Investigation of Transport Component Design Effect on a Proton Exchange Membrane Fuel Cell. J Power Sour, 2006, 160(1), 340-352.
19. ChJung H.M., Lee W.Y., Park J.S., Kim C.S. Numerical analysis of polymer electrolyte fuel cell. Int J Hydrog Energ, 2003, 29, 945–954.
20. Shimpalee S.W., Lee K., Van Zee J.W., Neshat H.N. Predicting the transient response of a serpentine flow-field PEMFC I. Excess of normal fuel and air. J Power Sour, 2006, 156(2), 355–368.
21. Weng F.B., Su A., Jung G.B., Chiu Y.C., Chan S.H. Numerical prediction of concentration and current distribution in PEMFC. J Power Sour, 2005, 145, 546–554.
22. Ahmed D.H., Sung H.J. Designs of a deflected membrane electrode assembly for PEMFCs. J Heat Mass Transf, 2008, 51, 327–339.
23. Arabi A., Roshandel R. Numerical modeling of an innovative bipolar plates design based on the leaf venation patterns for PEM fuel cells. Int J Eng, 2012, 25-3, 177-186.
24. Aiyejina A., Sastry M.K.S. PEMFC Flow Channel Geometry Optimization. J Fuel Cell Sci Tech, 2011, 9(1), 12-28.
25. Imanmehr S., Pourmahmod N. A Parametric Study of Bipolar Plate Structural Parameters on the Performance of Proton Exchange Membrane Fuel Cell. J Fuel Cell Sci Tech, 2012, 9, 1-9.
26. Fuller E.N., Schettler P.D., Giddings J.C. A new method for prediction of binary gas-phase diffusion coefficients. Ind Eng Chem, 1996, 58(5), 18-27.
27. Berning T., Lu D.M., Djilali N. Three-dimensional computational analysis of transport phenomena in a PEM fuel cell. J Power Sour, 2002, 106(1-2), 284-94.
28. Wang L., Husar A., Zhou T., Liu H. A parametric study of PEM fuel cell performances. Int J Hydrog Energy, 2003, 28(11), 1263-1272.